

Co-seismic landslide mapping following the 2023 El Haouz earthquake using differential interferometric synthetic aperture radar and optical imagery (High Atlas, Morocco)

Allal Labriki^{1*}, Yasmina Bouchatta², Karima Labriki^{3*},
Abderrahim Hassani⁴, Sara Zoraa¹, Saïd Chakiri⁴, Abdelkhalek Ghazi³

¹ Laboratory of Geosciences, Geomatics, and Environment (L2GE), Faculty of Sciences Ben M'Sik, Hassan II University, P.O. Box 7955, Casablanca, Morocco

² Faculty of Sciences and Techniques of Al Hoceima, Abdelmalek Essaâdi University, P.O. Box 34, Ajdir 32003 Al Hoceima, Morocco

³ Territory, Environment and Development Laboratory, Faculty of Humanities and Social Sciences, Ibn Tofail University, P.O. Box 242, Kenitra, Morocco

⁴ Geosciences Laboratory, Faculty of Sciences, Ibn Tofail University, B.P. 133, 14000 Kenitra, Morocco

* Corresponding author's e-mail: labriki.allal@gmail.com

ABSTRACT

The Mw 6.8 El Haouz earthquake of September 8, 2023, triggered extensive co-seismic mass movements in the Moroccan High Atlas. This study presents the first comprehensive inventory and spatial analysis of slope instabilities associated with this event. Using an integrated approach based on differential interferometric synthetic aperture radar (DInSAR) and high-resolution optical imagery, we identified both low-displacement slope deformations and large-scale rockfalls throughout the affected region. Visual interpretation and mapping of displacement anomalies observed in the DInSAR data, supported by a high-resolution digital elevation model (DEM), enabled the identification of over 570 low-displacement slope movement events, including shallow landslides, slope deformations, debris flows, and gravitational failures affecting pop-up structures. These movements deviate from the dominant tectonic displacement pattern and reveal the presence of widespread shallow instabilities. In parallel, analysis of high-resolution optical imagery led to the mapping of 1,203 co-seismic rockfalls, with individual areas ranging from 113.54 m² to 1.62 km², covering a cumulative surface of 66.03 km². Spatial analysis indicates that the majority of these events occurred in areas characterized by intense ground motion and steep slopes. This study fills a critical knowledge gap by documenting the multiscale geomorphic impacts of co-seismic mass movements in the Atlas Mountains. The results underscore the value of combining radar and optical remote sensing for seismic hazard assessment and provide key inputs for regional risk mitigation and terrain stability analysis.

Keywords: DinSAR technology, surface displacements, co-seismic landslides, Al-Haouz earthquake, Moroccan High Atlas.

INTRODUCTION

Morocco, located at the convergence of the African and European tectonic plates, experiences high seismic activity and is exposed to risks with potentially devastating consequences (El Mrabet, 1999; Cherkaoui et al., 1991, 2017). On September 8, 2023, at 10:11 PM, a Mw 6.8 (as reported by the USGS - United States Geological

Survey) earthquake struck the Al Haouz region, marking one of the most significant seismic events in recent decades. The epicenter of this major tremor was pinpointed by the Moroccan Geophysical Institute in the commune of Ighil, Al-Haouz province, approximately 70 kilometers southwest of Marrakech. The human toll was tragic, with nearly 3.000 fatalities and over 5.500 injuries. Beyond the immediate damage caused

by seismic shaking, the earthquake triggered a series of gravitational movements, including landslides, rockfalls, block collapses, and cliff failures, which further intensified the devastating impact on infrastructure and local communities.

The geomechanical evolution of rock masses under seismic activity plays a major role in triggering gravitational movements (Fellah et al., 1996; Labriki et al., 2019). Earthquakes induce structural changes within rocks, notably through increased fracturing and displacements along active faults. These seismic movements lead to a redistribution of internal stresses, weakening the rock mass's mechanical properties and potentially causing gradual or immediate ruptures. Over time, the accumulation of these disturbances reduces slope stability, making rock masses more vulnerable to landslides, especially in tectonically active regions (Keefer, 1984; Azzouz et al., 2002; Sassa et al., 2007; Havenith and Bourdeau, 2010; Labriki et al., 2019).

Although the Mw 6.8 El Haouz earthquake that struck the High Atlas region on 8 September 2023 was one of the most powerful seismic events recorded in Morocco in recent decades, no systematic study has yet examined the spatial distribution and characteristics of the co-seismic slope failures it triggered. This lack of documentation is scientifically significant, given the well-known role of such gravitational processes in amplifying seismic damage, particularly in structurally complex and mountainous environments. In contrast to other tectonically active regions such as the Himalayas, Japan, or the Andes, where co-seismic landslides are routinely inventoried and analyzed following major earthquakes, comprehensive post-event assessments remain scarce in the Moroccan context. This gap limits both the understanding of regional slope dynamics under seismic stress and the development of accurate hazard scenarios. The El Haouz earthquake therefore presents a unique opportunity to investigate how strong ground motion interacts with lithological, topographic, and structural factors to produce slope instabilities across a variety of geological settings.

The present study aims to establish the first detailed inventory of gravitational movements associated with the 2023 El Haouz earthquake and to analyze their spatial distribution in relation to key geological and geomorphological controls. In doing so, it contributes to a better understanding of the seismic response of mountain slopes in the Atlas

range and provides critical insights to improve seismic hazard assessment in Morocco (Nouayti et al., 2024; Ziraoui et al., 2024), a country increasingly exposed to the combined impacts of tectonic and hydro-climatic risks (Khaddari et al., 2023; El Idrissi et al., 2024; Rahoui et al., 2024).

GEOLOGICAL CONTEXT

The study area, located in the eastern part of the Western High Atlas, is characterized by complex tectonics resulting from the inversion of the Mesozoic rift within the framework of Africa-Europe convergence (Poisson et al., 1998; Beauchamp et al., 1999; Frizon de Lamotte et al., 2000; Ayarza et al., 2005; Ellero et al., 2012; Domènech et al., 2015). This tectonic activity, which has deeply influenced the current structure of the mountain range, has reactivated ancient Mesozoic structures as well as major faults inherited from the Variscan orogeny (Proust, 1973; Petit, 1976; Piqué and Laville, 1993; Morel et al., 2000) (Figure 1). Additionally, this reactivation segmented the basement into overlapping blocks, resulting in a double-verging mountain chain with a structural style characterized by “pop-up” dome formations (Domènech et al., 2015; Fekkak et al., 2018). The evolution of this compressive tectonics, which began in the Middle Miocene and continued into the Quaternary, has shaped the steep reliefs across the entire region (Mattauer et al., 1977). The faults and discontinuities created within this tectonic framework weaken the cohesion of rock masses, making slopes particularly vulnerable during seismic events.

The study area, located within the Paleozoic massif of the Western High Atlas (Figure 1 and 2), is characterized by a lithology dominated by metamorphic and magmatic formations. Paleozoic schists, in particular, represent the main metamorphic formations, varying in composition and degree of metamorphism (Moret, 1931; Ouanaimi, 1989; Labriki, 1996; El Archi et al., 2004). Magmatic rocks in the area mainly include granites, diorites, dolerites, andesites, and rhyolites (El Archi et al., 2004; Chacrone and Hamoumi, 2005). To the north, these crystalline terrains are generally overlain by Meso-Cenozoic cover sequences, primarily comprising limestones, marls, sandstones, and conglomerates (Hafid et al., 2006; Fekkak et al., 2018). These rocks, often fractured and fragmented, are

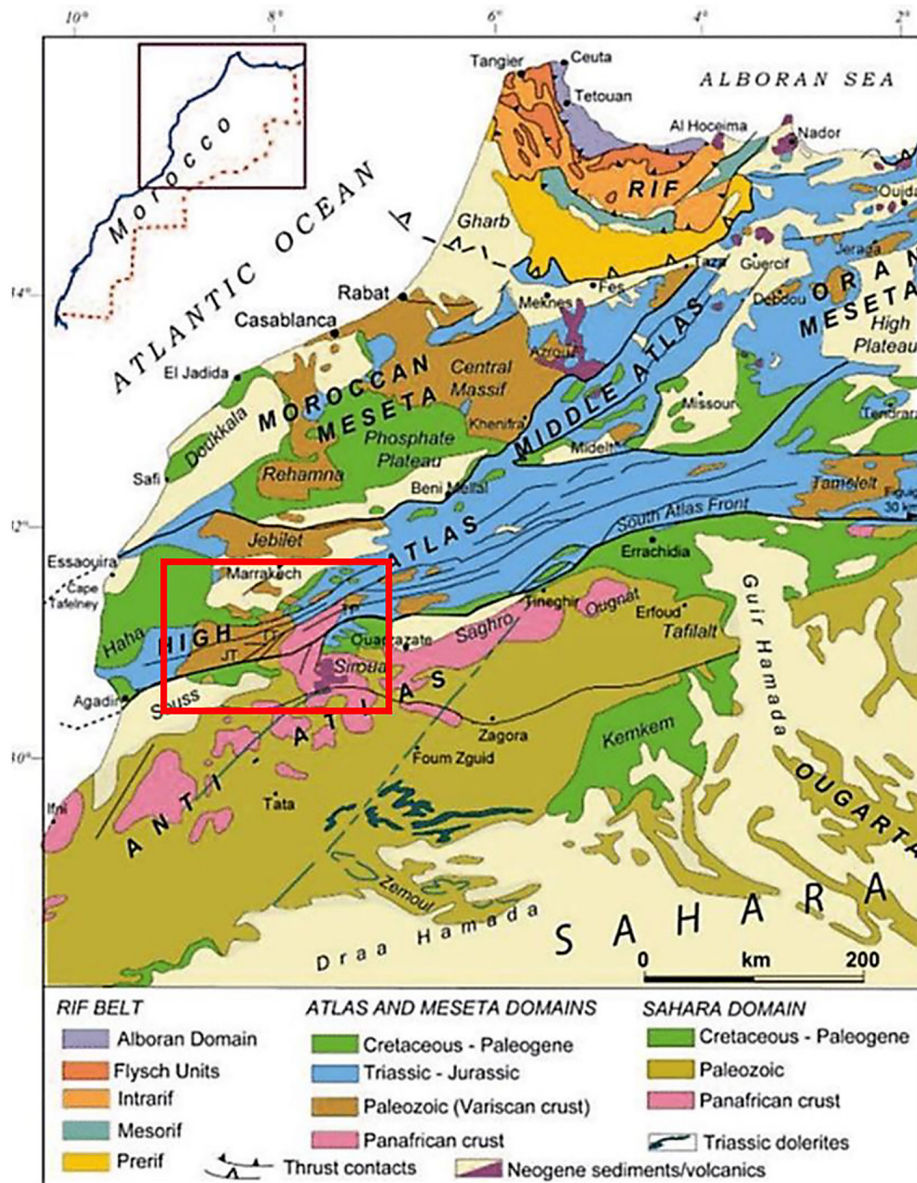


Figure 1. The structural domains of Morocco (Michard, 1976), red rectangle depicts the study area

particularly susceptible to gravitational movements, which are intensified by seismic tremors.

METHODOLOGY

The methodology adopted in this study follows a technical approach to determine both gravitational and tectonic surface deformation caused by the earthquake in the Al Haouz region. The process involved several key steps:

Interferogram creation

To monitor ground surface deformation following the September 8, 2023, earthquake, radar

interferometry was implemented. An ascending pair of Sentinel-1 radar images (Figure 2) (Table 1), captured before and after the earthquake (September 3, 2023, and September 15, 2023), was used for this analysis. Our analysis is based on Sentinel-1 TOPS (Terrain Observation with Progressive Scans) data to investigate co-seismic ground deformation through radar differential interferometry (DInSAR) (Jiun-Yee Yen et al., 2008; He et al., 2018).

The interferometric processing was carried out using the ESA SNAP software (version 9.0.0), which provided a comprehensive framework for handling the various stages of DInSAR data analysis (Figure 3).

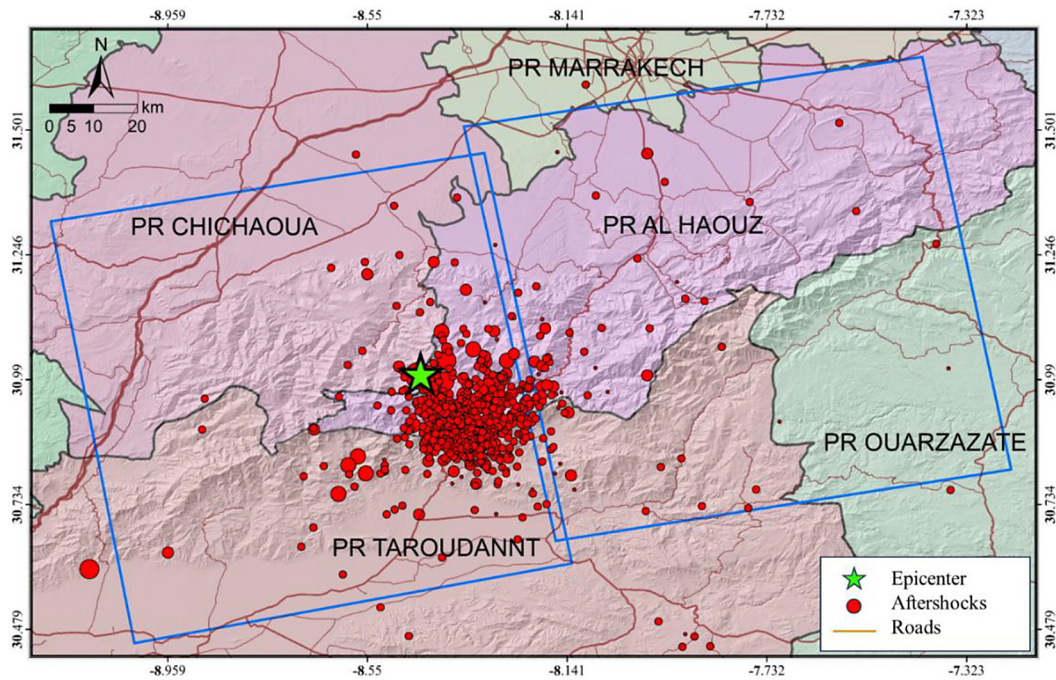


Figure 2. Geographic setting map surrounding the 2023 Al Haouz Mw 6.8 earthquake. Blue rectangles indicate the footprints of the Sentinel-1 images used in this study, and red spheres show the distribution of aftershocks

Table 1. Interferometry pair used in this study (sentinel SAR data download from <https://browser.dataspace.copernicus.eu>, accessed in April 2024)

Satellite	Pass	Rel-Orbit	Master yyyymmdd	Slave yyyymmdd	Time interval days
Sentinel-1 A	Ascending	45	20230903	20230915	12

Precise image co-registration – extremely precise co-registration of the radar images was performed to ensure reliable measurements (De Zan and Guarnieri, 2006; Davidson et al., 2013; Xu, 2020). This step is crucial to minimize errors due to misalignment between pre- and post-earthquake images;

Interferogram generation – the interferogram was generated by subtracting the flat Earth phase and the topographic phase, highlighting the deformations associated with the earthquake;

Phase filtering – the phase filtering method of Goldstein and Werner (1998), was applied to reduce residuals and improve the quality of the interferogram. However, the low interferometric coherence, due to the region’s complex topography and dense vegetation (Michaelides et al., 2019; Ansari et al., 2020), limited the accuracy of the results;

Low-pass filter resampling – to mitigate the effects of low coherence, resampling using low-pass filtering was applied (Scott et al., 2017),

which allowed for data smoothing and improved deformation detection.

Calculation of surface deformation

After exploring and analyzing the interferogram, displacements were calculated from the interferometric phase to quantify the spatial deformations related to the Al Haouz earthquake (Figure 3). To resolve phase ambiguities, the SNAPHU algorithm (version 2.0.4) (Statistical-Cost Network-Flow Algorithm for Phase Unwrapping) was used (Chen and Zebker, 2000, 2001). This algorithm applies a maximum a posteriori (MAP) estimation to reliably unwrap the phase. The line of sight (LOS) displacement was then converted into a relative ground displacement map. This map was geocoded using the ‘Range Doppler Terrain Correction’ method with an SRTM digital elevation model (DEM) (Small et al., 2022). Finally, the displacement map was resampled to a 100 m resolution to enhance the detection of large-scale gravitational deformations,

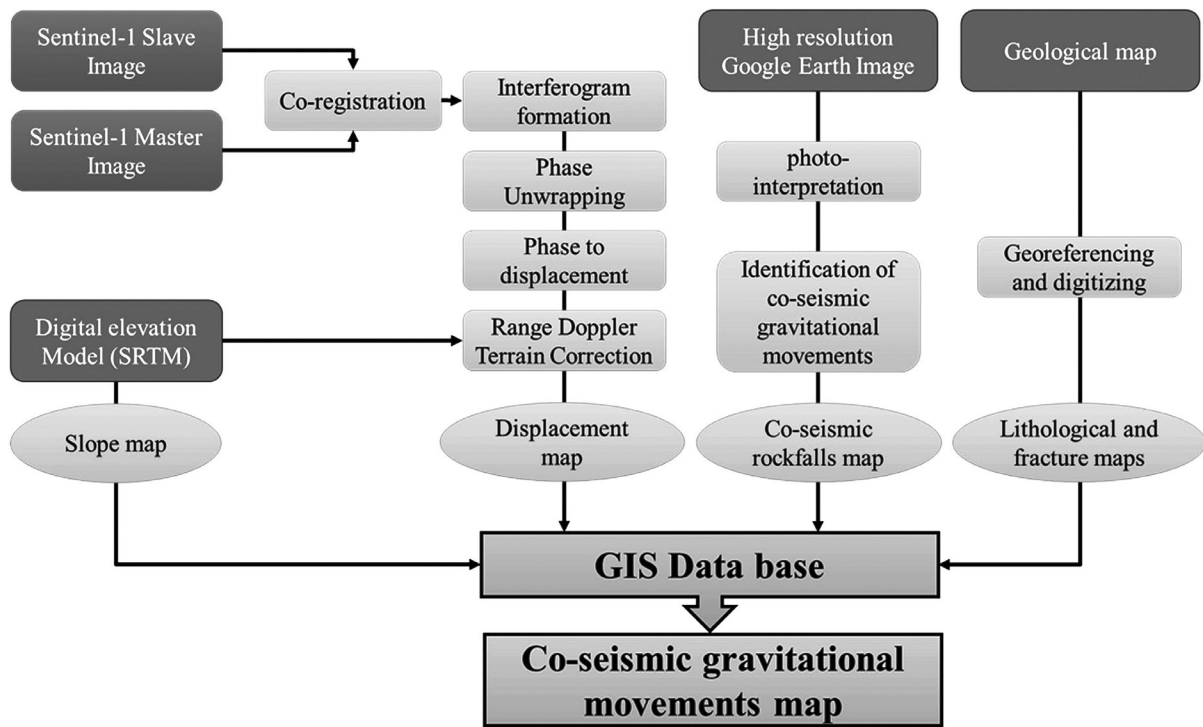


Figure 3. Flowchart illustrating the methodology used for mapping co-seismic gravitational movements, such as landslides and rockfalls, based on DInSAR data interpretation and high-resolution Google Earth imagery

while minimizing the influence of small, localized surface changes. This spatial resolution enables a clearer interpretation of regional deformation patterns by filtering out high-frequency noise and superficial displacements that are not significant for the applied methodological approach. Furthermore, in mountainous terrain, such resampling helps mitigate decorrelation effects, commonly associated with steep topography and dense vegetation, thereby improving the overall coherence and reliability of the interferometric signal.

Co-seismic and low-displacement slope movements

For the identification of co-seismic gravitational processes with emphasis on low-displacement slope failures, our approach is based on the analysis of displacement maps generated using the DInSAR technique. After producing these maps, we sought to distinguish gravitational displacements from tectonic deformation induced by the earthquake. Co-seismic low-magnitude movements were defined as localized displacement anomalies, clearly separated from the broader, continuous ground deformation associated with the seismic event. These anomalies typically reflect discrete surface responses, such as

differential ground motion, large surface breaks, or subtle slope deformations, which significantly deviate from the general deformation pattern. Their identification was based on the analysis of interferometric displacement maps, with particular attention to areas marked by abrupt displacement jumps, discontinuities, or localized patterns characteristic of gravitational slope deformation. Once detected, these anomalies were manually digitized with high spatial precision and incorporated into a geographic information system (GIS) to support spatial analysis, mapping, and interpretation within structural and geomorphological frameworks (Figure 3).

Co-seismic rockfalls with large displacements

Furthermore, the identification of rockfalls was carried out using high-resolution images from the Google Earth database (Figure 3). A visual photo-interpretation was performed based on images acquired after the Al Haouz earthquake on September 8, 2023. This process allowed us to rigorously detect and digitize the co-seismic rockfall movements triggered by the earthquake, through a systematic comparison of pre- and post-event images. In several cases, the identification of these features on interferometric displacement

maps was limited due to loss of coherence caused by large rockfall displacements, which exceeded the detection capabilities of DInSAR. To address this limitation, Google Earth Pro was used as a complementary tool for the visual identification and manual mapping of rockfall events. Clearly visible features -such as detachment zones, run-out paths, and impact areas- were digitized using high-resolution optical imagery, then exported as KML files and integrated into our GIS database for further spatial and structural analysis.

RESULTS

DInSAR and displacement data

The interferogram obtained in this study highlights a co-seismic deformation field characteristic of compressive movements (Figure 4). This earthquake exerted a notable influence on the Paleozoic massif of the western High Atlas, which is structured into three distinct zones: the axial zone and the northern and southern sub-Atlas zones, segmented by longitudinal faults (Mustaphi et al., 1997; Hafid et al., 2006; Domènech et al., 2016; Fekkek et al., 2018). The alignment of patterns observed in the interferogram with the local fault

network suggests that the Al Haouz earthquake could be linked to the reactivation of pre-existing tectonic structures. Concentric fringes indicate differential uplift in a compressive context, with a significant impact on the axial zone.

The displacement map, generated from the co-seismic interferogram, provides a detailed representation of the tectonic deformations that occurred during the earthquake, with uplift exceeding 20 cm (LOS) around the seismic focus. This recorded uplift is directly related to the observed compressive movements, reflecting a large-scale tectonic readjustment in this part of the western High Atlas. Consequently, this vertical motion triggered co-seismic gravitational movements, affecting the entire deformation zone. Thus, the displacement map not only shows the general tectonic uplift but also reveals the complexity of interactions between tectonic and gravitational processes in a region particularly sensitive to co-seismic movements.

These co-seismic low-displacement slope movements are expressed as localized anomalies that deviate from the broader ground deformation pattern visible in the interferometrically derived displacement map (Figure 5). While the overall displacement field primarily reflects

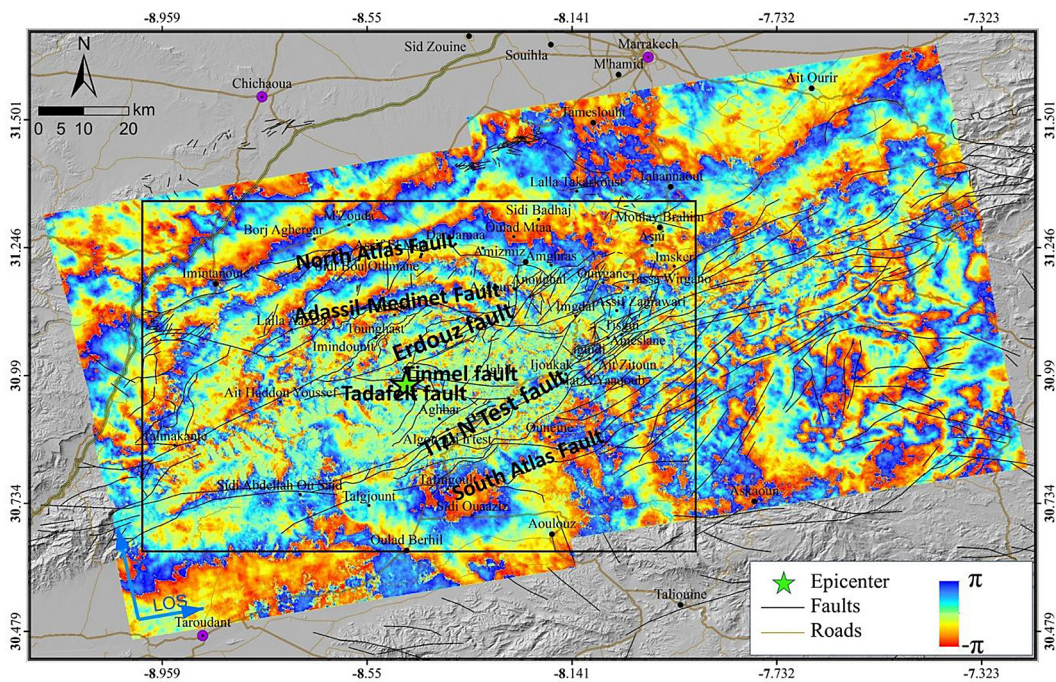


Figure 4. Interferogram obtained from ascending Sentinel-1 data illustrating the co-seismic deformation induced by the Al Haouz Mw 6.8 earthquake (08-09-2023). The colored fringes depict ground surface displacements, with each fringe corresponding approximately to 2.8 cm of displacement, providing a detailed view of the co-seismic effects on the region

regional crustal shortening associated with compressive tectonic forces, these localized deviations are indicative of gravitational instabilities, such as slope creep, lateral spreading, or shallow landslides, triggered by the sudden redistribution of subsurface stresses during seismic shaking (Figure 5a–c). The occurrence of these phenomena, often concentrated along steep slopes and near active fault zones, illustrates that

seismic deformation does not affect the landscape uniformly. Instead, it interacts differently with geological structures depending on factors such as lithology, structural orientation, degree of fracturing, and the mechanical predisposition of slopes to failure. This underscores the need to account for both regional tectonic settings and local slope conditions when assessing co-seismic landslide susceptibility.

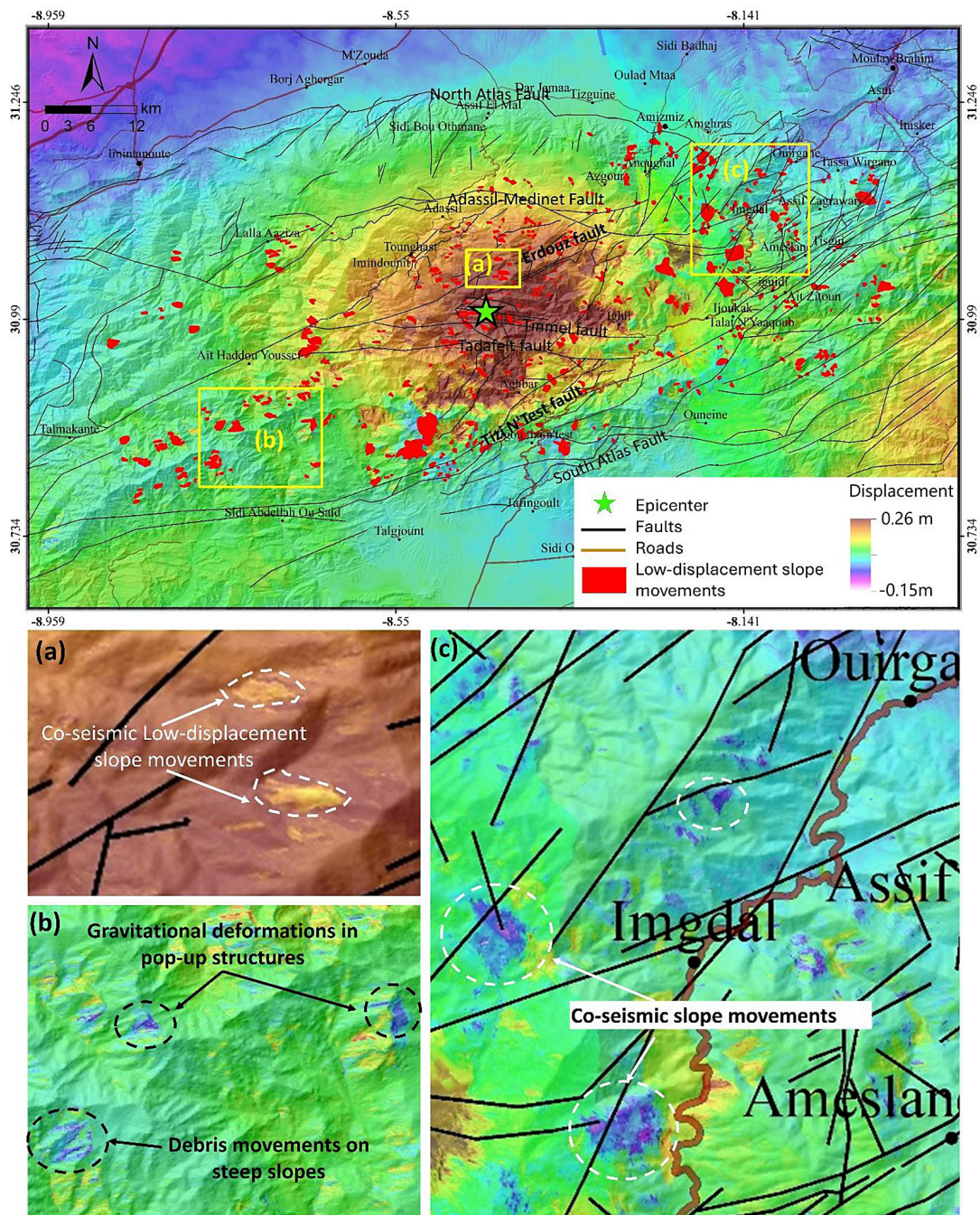


Figure 5. Co-seismic displacement map derived from previous interferometric data, showing displacements in meters with a color legend for interpreting variations. This map highlights several displacement anomalies related to co-seismic gravitational deformations: (a) low-displacement slope movements; (b) gravitational deformations in pop-up structures; (c) large co-seismic slope deformations

To advance this analysis, we identified and manually digitized co-seismic low-displacement slope movements based on localized anomalies observed in the displacement map. By combining this map with a high-resolution digital elevation model (DEM), we were able to accurately highlight subtle slope deformation patterns that deviate from the dominant tectonic displacement induced by the earthquake. This integrated approach enabled the identification of over 570 distinct co-seismic low-displacement slope movement events distributed throughout the mountainous region. These movements include shallow landslides (Figure 5a), slope deformations (Figure 5c), debris flows, and gravitational instabilities affecting pop-up structures (Figure 5b), all of which contributed to amplifying the earthquake's impact on both the landscape and local infrastructure.

High-resolution Google Earth data

To identify co-seismic rockfalls triggered by the Al Haouz earthquake, we utilized high-resolution pre- and post-seismic images from Google Earth's historical database, selecting images captured just before and immediately after the seismic event to enable effective comparison.

Visual analysis was conducted by closely examining areas prone to rockfalls, focusing on steep slopes, mountainous regions, and cliffs (Figure 6 and 7). We identified indicators of rockfalls such as changes in vegetation (despite the sparse vegetation in our study area), the appearance of scars in the form of light-colored marks on slopes indicative of landslides, accumulation of debris on roads, at the base of slopes, or in riverbeds, and variations in soil color due to the exposure of new surfaces (Figure 6 and 7). By comparing images before and after the earthquake, we detected differences and noted changes indicative of rockfalls. Affected areas were documented using markers for identification. To map these co-seismic rockfalls, we employed the "Polygon" tool in Google Earth Pro to delineate the rockfall areas. The data were saved and exported with relevant descriptions, dates, and annotations to create a GIS database for further analysis and interpretation.

The analysis revealed a total of 1.203 rockfalls, with areas ranging from 113.54 m² to 1,619,947.45 m², resulting in a cumulative affected area of 66,025,704.5 m². The average rockfall

area was 54,884.20 m², with a standard deviation of 138,350.02 m², highlighting significant variability in the size of observed rockfalls. This variability suggests that the earthquake impacted areas at various scales, from small superficial slides to large, massive rockfalls.

This study demonstrates that the rockfalls induced by the earthquake are primarily concentrated in areas with a high density of tectonic faults and on steep slopes, indicating a close relationship between geological structures, terrain topography, and susceptibility to rockfalls. During the Al Haouz earthquake, rockfalls typically initiated at ridge crests, emphasizing the importance of local topographic conditions. The affected areas are predominantly composed of highly fractured Paleozoic rocks. This geological fragility, combined with mechanical and chemical weathering, increases the likelihood of rockfalls during seismic shaking. Therefore, it is crucial to consider both geological and topographic factors when assessing co-seismic rockfall risk and improving hazard management in seismically active regions.

DISCUSSION

Earthquake induced landslides are major geological hazards that pose significant risks to infrastructure and populations in tectonically active regions. Earthquakes and rainfall are the primary triggers for these phenomena, as they significantly increase pore pressure in fractures and voids, thereby reducing material cohesion (e.g., Sassa et al., 2007). For example, the 2018 Hokkaido Eastern Iwate earthquake in Japan highlighted the risk of recurrence and development of shallow landslides in seismic zones (Yoshihara et al., 2023). Furthermore, due to micro-relief effects, specific parts of slopes are more likely to be affected by external forces such as earthquakes (Meunier et al., 2008; Fan et al., 2019; Dai et al., 2023). Typically, earthquakes with magnitudes greater than 4 are widely recognized for their potential to trigger landslides (e.g., Keefer, 1984; Havenith and Bourdeau, 2010). Identifying co-seismic deformations induced by earthquakes is essential for understanding and mitigating these risks. Radar differential interferometry (DInSAR) has proven to be an effective tool for mapping surface displacements associated with both tectonic and gravitational movements (Notti et al., 2014; Intrieri et al., 2017; Del Soldato et al., 2019; Aslan

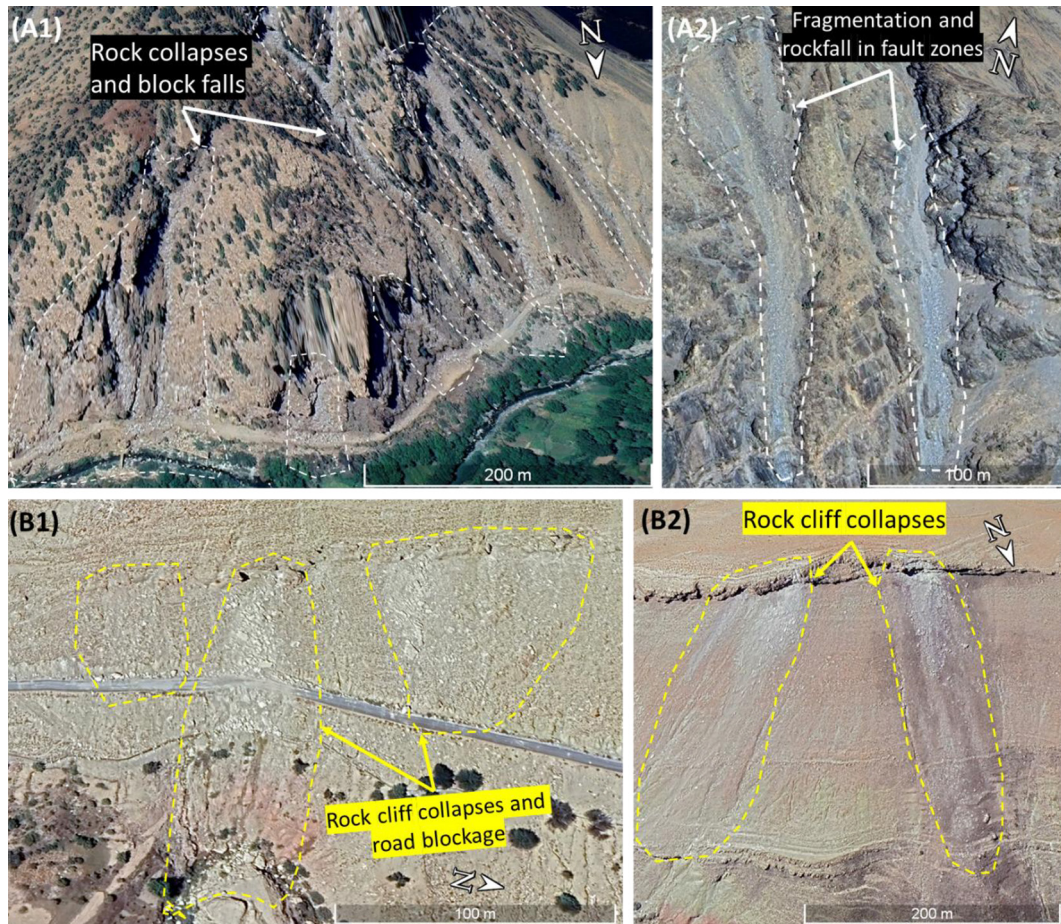


Figure 6. Examples of rockfalls and rock collapses triggered by the Al Haouz earthquake, observed in Google Earth images dated 09/19/2023, 10 days after the earthquake (see location in Figure 8, zones A and B). (A1) Rockfalls and collapses in the rural commune Aghbar (Lat=30°53'32.77"N; Long=8°29'20.09"W); (A2) Rockfalls in a fault zone (Lat=30°54'41.75"N; Long=8°28'11.13"W); (B1) Cliff collapse blocking the road near Ighermane village, Chichaoua province (Lat=31°8'58.71"N; Long=8°26'7.50"W); (B2) Cliff collapse (Lat=31°9'11.79"N; Long=8°23'57.78"W)

et al., 2020; Bekaert et al., 2020). By analyzing DInSAR data, it is possible to detect and characterize the extent of co-seismic deformations, which informs risk assessments and guides disaster response efforts.

In this context, the analysis of DInSAR data and displacement measurements shows that the Al Haouz earthquake generated three distinct types of movements contributing to the observed co-seismic deformation in the region. First, a tectonic uplift of up to 20 cm in a compressive context affected the entire axial zone surrounding the earthquake (Huang et al., 2024; Bao et al., 2025). This uplift results from the reactivation of deep compressive faults, leading to significant vertical ground displacement (Figure 5). Second, low-displacement gravitational movements were observed (Figure 9a-c), affecting soft formations on medium to steep slopes, primarily composed of Paleozoic rocks.

These movements concentrate in areas of high tectonic deformation, where weakness planes such as fracturing, schistosity, and stratification facilitate the formation of slip surfaces during seismic shaking. Third, rapid gravitational movements, including rockfalls, cliff collapses, Blocks and Boulder falls, were triggered (Figure 7 and Figure 9d-i). Similar to movements observed in sandstone, siltstone, and granite formations during the May 12, 2008, Wenchuan earthquake in China (Xu et al., 2014), the Al Haouz earthquake primarily affected geologically fractured and fragmented formations, including metamorphic and magmatic rocks as well as the Upper Cretaceous Imi N'Tala limestone formations (Figure 7). These slope movements predominantly occur along steep bedrock escarpments, underscoring the critical role of topographic factors in controlling slope stability during seismic events. High slope gradients amplify the downslope



Figure 7. The tragic co-seismic collapse of massive rock formations onto the village of Imi N'Tala (see location in Figure 8, zone c, Lat= 31° 7'44.85"N; Long= 8°16'4.30"O), resulting in the deaths of more than 80 people; (a) Google Earth image taken before the earthquake on 28 December 2022 ; (b) Google Earth image taken only five days after the earthquake on 14 September 2024, showing the total destruction of the village caused by the collapse of Upper Cretaceous limestone formations at Imi N'Tala; (c and d) two photographs of this collapse, illustrating the extent and magnitude of the event

gravitational force component (Labriki et al., 2020; Ajraoui et al., 2025; Labriki et al., 2025), thereby increasing the likelihood of failure and promoting the detachment of unstable rock masses near ridgelines and crests (Figure 9f, g and i). Furthermore,

the spatial distribution of these movements is strongly associated with zones of high fault density and intense rock mass fracturing, which reduce material cohesion and create preferential pathways for failure initiation.

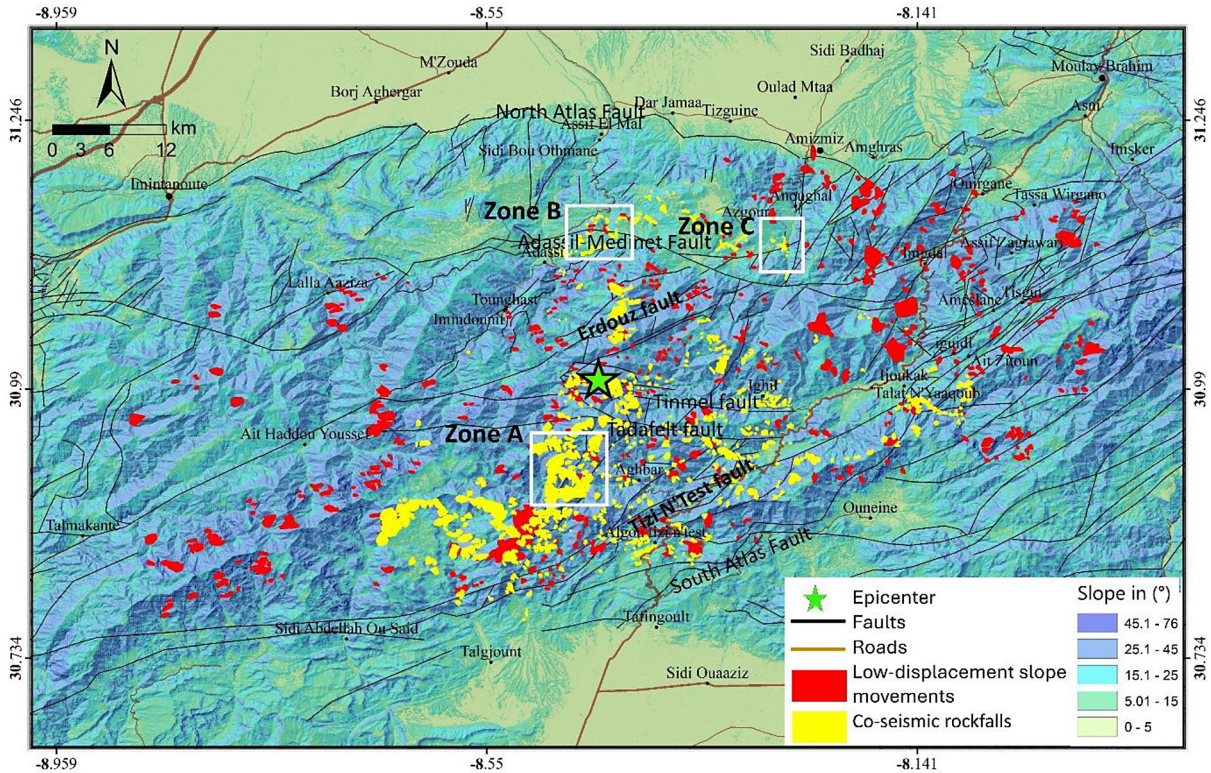


Figure 8. Spatial distribution map of rockfalls and low-displacement slope movements induced by the Al Haouz earthquake, overlaid on a background representing the relief, slope, and main fault network of the region

The spatial distribution map of co-seismic gravitational movements (Figure 8), derived from the integration of slope gradients, fault networks, and manually digitized landslide inventories, provides clear evidence of the topographic and structural controls influencing slope failures triggered by the Al Haouz earthquake. The map shows that both low-displacement slope movements and large co-seismic rockfalls are primarily concentrated along steep ridgelines, often near fault intersections or in zones of highly fractured rock masses. This distribution pattern emphasizes the importance of local slope geometry and tectonic structure in the initiation of gravitational instabilities. In contrast to the findings reported by Lanxin Dai during the September 5, 2022 Luding earthquake in Sichuan-China, where small landslides were mainly concentrated at the base of slopes, our results indicate that failures in the Al Haouz region predominantly originated near the crests. This contrast underscores the role of morpho-structural setting in shaping the spatial behavior of co-seismic landslides, particularly in regions of high relief such as the central High Atlas. These insights highlight the need to integrate slope morphology, litho-structural conditions,

and seismotectonic context into any regional landslide hazard assessment.

Furthermore, the distribution of seismic energy during the Al Haouz earthquake was largely concentrated in the axial mountainous zone of the study area (Huang et al., 2024; Bao et al., 2025). This energy was primarily dissipated along major tectonic structures, including active faults and pop-up features, which accommodated the bulk of the deformation. The concentration of strain in these zones facilitated the triggering of gravitational movements, especially on steep slopes and along fault traces, through mechanisms such as shearing, mechanical disintegration, grain-size reduction, and dilatancy-related weakening (Labriki et al., 2019). These processes highlight how topographic steepness and geological conditions, when combined with intense seismic loading, enhance material fragmentation and significantly increase the likelihood of slope failure (e.g., Fellaoui et al., 1996; Azzouz et al., 2002; Labriki et al., 2019). A striking example of this multi-factor interaction is the catastrophic rockfall that occurred in the village of Imi N'Tala (Figure 7), where the collapse of massive rock blocks led to the loss of more than 80 lives.



Figure 9. Field observations of coseismic gravitational processes triggered by the Al Haouz earthquake in the central High Atlas: (a–d) cracks, lateral displacements, and rockfalls observed in the commune of Ighil (epicentral area); (e) rockslide and road collapse in Idaghassen village; (f) boulder fall near Imi N’Ouzrou village; (g) large boulder fall in Tilikente village, Talkjounte commune; (h) co-seismic rockfall impact on a vehicle along the Talat N’Yaaqoub road; (i) boulder fall blocking the Oukaimeden road

CONCLUSIONS

This study provides new insights into the spatial distribution and characteristics of co-seismic gravitational movements triggered by the 2023 El Haouz earthquake in the Moroccan High Atlas. Through the integration of DInSAR data and high-resolution image analysis, we were able to detect both high-magnitude slope failures and subtle, low-amplitude displacements often overlooked by conventional methods. This dual-scale inventory constitutes the first spatially explicit mapping of co-seismic gravitational processes in this region, filling a significant gap in the understanding of their role as amplifiers of seismic hazard. The findings highlight several distinctive characteristics of these gravitational responses:

- Systematic downslope movement along gravitational vectors, contrasting with tectonic uplift;
- Triggering by seismic ground shaking, especially on medium to steep slopes;
- Formation of fractures and surface ruptures that may evolve into future landslide planes;
- A wide range of displacement magnitudes, from millimetric motions in soft terrains to large, rapid mass movements in consolidated rock units.

By addressing the overlooked contribution of co-seismic slope instabilities to seismic risk, this study contributes to a more comprehensive understanding of earthquake-induced surface processes in intracontinental mountain belts. It opens important prospects for improving seismic hazard management, including land-use planning, infrastructure reinforcement, and risk communication. The results also underscore the relevance of developing early warning systems and predictive models that integrate co-seismic mass movements into broader seismic risk reduction frameworks.

REFERENCES

1. Ajraoui, A., Chakiri, S., Mansouri, H., Ben Haddou, M., Laassilia, O., Labriki, A., Soufi, A. (2025). Geotechnical analysis and stabilization of the Jebha landslide: A case study from Morocco's Mediterranean Ring Road. *Civil Engineering and Architecture*, 13(2), 949–964. <https://doi.org/10.13189/cea.2025.130214>
2. Ansari, H., De Zan, F., Parizzi, A. (2020). Study of systematic bias in measuring surface deformation with SAR interferometry. *IEEE Transactions on Geoscience and Remote Sensing*, 59(2), 1285–1301.
3. Aslan, G., Foumelis, M., Raucoules, D., de Michele, M., Bernardie, S., Cakir, Z. (2020). Landslide mapping and monitoring using persistent scatterer interferometry (PSI) technique in the French Alps. *Remote Sens*, 12(8), 1305. <https://doi.org/10.3390/rs12081305>
4. Ayarza, P., Alvarez-Lobato, F., Teixell, A., Arbolea, M. L., Tesón, E., Julivert, M., Charroud, M. (2005). Crustal structure under the central High Atlas Mountains (Morocco) from geological and gravity data. *Tectonophysics*, 400, 67–84.
5. Azzouz O., El Fellah B., Chalouan, A. (2002). Processus de glissement dans le Massif de Bokoya (Rif interne, Maroc): exemple de Cala Bonita. *Bulletin Institut scientifique., Section Sciences de la Terre*, 24, 33–40.
6. Bao, M., Abdelaal, M. I., Saleh, M., Chourak, M., Mohamed, M., Xing, M. (2025). Unlocking the hidden secrets of the 2023 Al Haouz earthquake: Coseismic model reveals intraplate reverse faulting in Morocco derived from SAR and seismic data. *International Journal of Applied Earth Observation and Geoinformation*, 137, 104420. <https://doi.org/10.1016/j.jag.2025.104420>
7. Beauchamp, W., Allmendinger, R. W., Barazangi, M., Demnati, A., El Alji, M., Dahmani, M. (1999). Inversion tectonics and the evolution of the High Atlas Mountains, Morocco, based on a geological-geophysical transect. *Tectonics*, 18, 163–184.
8. Bekaert, D. P., Handwerker, A. L., Agram, P., Kirschbaum, D. B. (2020). InSAR based detection method for mapping and monitoring slow-moving landslides in remote regions with steep and mountainous terrain: An application to Nepal. *Remote Sens of Environ*, 249, 111983. <https://doi.org/10.1016/j.rse.2020.111983>
9. Chacrone, C., Hamoumi, N. (2005). L'Arenig-Llanvirn du Haut Atlas occidental et central (Maroc). Environnements sédimentaires, paléogéographie et contrôle de la sédimentation. *Comptes Rendus Geosciences* 337, 1026–1034.
10. Chen, C.W., Zebker, H.A. (2000). Network approaches to two-dimensional phase unwrapping : intractability and two new algorithms. *JOSA A*, 17(3), 401–414.
11. Chen, C.W., Zebker, H.A. (2001). Two-dimensional phase unwrapping with use of statistical models for cost functions in nonlinear optimization. *JOSA A*, 18(2), 338–351.
12. Cherkaoui, T.E. (1991). *Contribution à l'étude de l'aléa sismique au Maroc*. Thèse Doctorat, Université de Grenoble, France, 246.
13. Cherkaoui, T.E., Medina, F., Mridekh, A. (2017).

- Reevaluación de los parámetros del sismo mayor de Fez del 11 de mayo de 1624. *Física De La Tierra*, 29, 135–157. <https://doi.org/10.5209/FITE.57469>
14. Dai, L., Fan, X., Wang, X. (2023). Coseismic landslides triggered by the 2022 Luding Ms6.8 earthquake, China. *Landslides*, 20, 1277–1292. <https://doi.org/10.1007/s10346-023-02061-3>
 15. Davidson, G., Mantle, V., Rabus, B., Williams, D., Geudtner, D. (2013). *Implementation of TOPS mode on RADARSAT-2 in support of the Sentinel-1 mission*. In Proc. ESA Living Planet Symposium 1–22.
 16. De Zan, F., Guarnieri, A.M. (2006). TOPSAR: Terrain observation by progressive scans. *IEEE Transactions on Geoscience and Remote Sensing*, 44(9), 2352–2360.
 17. Del Soldato, M., Solari, L., Poggi, F., Raspini, F., Tomás, R., Fanti, R., Casagli, N. (2019). Landslide-induced damage probability estimation coupling InSAR and field survey data by fragility curves. *Remote Sens*, 11(12), 1486. <https://doi.org/10.3390/rs11121486>
 18. Domènech, M., Teixell, A., Babault, J., Arboleya, M.L. (2015). The inverted Triassic rift of the Marrakech High Atlas: A reappraisal of basin geometries and faulting histories. *Tectonophysics*, 663, 177–191. <https://doi.org/10.1016/j.tecto.2015.03.017>
 19. Domènech, M., Teixell, A., Stockli, D. F. (2016). Magnitude of rift-related burial and orogenic contraction in the Marrakech High Atlas revealed by zircon (U-Th)/He thermochronology and thermal modeling. *Tectonics*, 35, 2609–2635. <https://doi.org/10.1002/2016TC004283>
 20. El Arch, i A., El Houicha, M., Jouhari, A., Bouabdelli, M. (2004). Is the Cambrian basin of the Western High Atlas (Morocco) related either to a subduction zone or a major shear zone? *Journal of African Earth Sciences*, 39, 311–318.
 21. El Idrissi, S., Zerdeb, O., Labriki, A., Mehdioui, S., El Omari, M., Chakiri, S., Inekach, S. (2024). Diachronic study of the North Atlantic Coast of Morocco between Larache and Moulay Bouselham: A geometric approach. *Ecological Engineering & Environmental Technology*, 25(6), 90–103. <https://doi.org/10.12912/27197050/186683>
 22. El Mrabet, T. (1999). *Histoire sismologique du Maroc*. Document de 3ème cycle, Faculté des Lettres, Université Mohammed V, Rabat, 375.
 23. Fan X., Scaringi G., Korup O., West A.J., van Westen C.J., Tanyas H., Hovius N., Hales T.C., Jibson R.W., Allstadt K.E. (2019) Earthquake-induced chains of geologic hazards: patterns, mechanisms, and impacts. *Rev Geophys* 57: 421–503 <https://doi.org/10.1029/2018RG000626>
 24. Fekkak, A., Ouanaimi, H., Michard, A., Soulaïmani, A., Ettachfini, E.M., Berrada, I., El Arabi, H., Lagnaoui, A., Saddiqi, O. (2018). Thick-skinned tectonics in a Late Cretaceous-Neogene intracontinental belt (High Atlas Mountains, Morocco): The flat-ramp fault control on basement shortening and cover folding. *Journal of African Earth Sciences*, 140, 169–188. <https://doi.org/10.1016/j.jafrearsci.2018.01.008>
 25. El Fellah B., Azzouz O., Asebriy L. 1996. Sikhad' Asfalou; exemple de glissement littoral sur la côte méditerranéenne de Bokoya entre Torrès et Bades (Rif, Maroc). *ORSTOM, réseau érosion, Bulletin 16*, 222–230.
 26. Frizon de Lamotte, D., Saint Bezar, B., Bracene, R., Mercier, E. (2000). The two main steps of the Atlas building and geodynamics of the western Mediterranean. *Tectonics*, 19, 740–761.
 27. Goldstein, R. M., Werner, C. L. (1998). Radar interferogram phase filtering for geophysical applications. *Geophysical Research Letters*, 25, 4035–4038.
 28. Hafid, M., Zizi, M., Bally, A.W., Ait Salem, A., 2006. Structural styles of the western onshore and offshore termination of the High Atlas, Morocco. *C. R. Geosci.* 338, 50–64.
 29. Havenith, H.-B., Bourdeau, C. (2010). Earthquake-induced hazards in mountain regions: A review of case histories from Central Asia. *Geologica Belgica*, 13, 135–150.
 30. Intrieri, E., Raspini, F., Fumagalli, A., Lu, P., del Conte, S., Farina, P., Allievi, J., Ferretti, A., Casagli, N. (2017). The Maoxian landslide as seen from space: Detecting precursors of failure with Sentinel-1 data. *Landslides*, 15(1), 123–133. <https://doi.org/10.1007/s10346-017-0915-7>
 31. He, P., Ding, K., Xu, C. (2018). The 2016 Mw 6.7 Aketao earthquake in Muji range, northern Pamir. *International Journal of Applied Earth Observation and Geoinformation*, 73, 99–106. <https://doi.org/10.1016/j.jag.2018.06.001>
 32. Huang, K., Wei, G., Chen, K., Zhang, N., Li, M., Dal Zilio, L. (2024). The 2023 Mw6.8 Morocco earthquake: A lower crust event triggered by mantle upwelling? *Geophysical Research Letters*, 51, e2024GL109052. <https://doi.org/10.1029/2024GL109052>
 33. Intrieri, E., Raspini, F., Fumagalli, A., Lu, P., del Conte, S., Farina, P., Allievi, J., Ferretti, A., Casagli, N. (2017). The Maoxian landslide as seen from space. *Landslides*, 15(1), 123–133. <https://doi.org/10.1007/s10346-017-0915-7>
 34. Jiun-Yee Yen, K.-S. Chen, C.-P. Chang, W.-M. Boerner. (2008). Evaluation of earthquake potential and surface deformation by Differential Interferometry. *Remote Sensing of Environment*, 112(3), 782–795. <https://doi.org/10.1016/j.rse.2007.06.012>
 35. Keefer, D. K. (1984). Landslides caused by earthquakes. *Geol Soc Am Bull*, 95, 406–421.

36. Khaddari, A., Jari, A., Chakiri, S., El Hadi, H., Labriki, A., Hajaj, S., et al. (2023). A Comparative analysis of analytical hierarchy process and fuzzy logic modeling in flood susceptibility mapping in the Assaka Watershed, Morocco. *Journal of Ecological Engineering*, 24(8), 62–83. <https://doi.org/10.12911/22998993/165958>
37. Labriki, A., Bouchatta, Y., Labriki, K., Zriouel, F., El Hilali, M., Chafiq, T., Chakiri, S., Ghazi, A. (2025). Morphodynamic analysis and identification of triggering mechanisms of flow-like landslides in the Trougoût torrential watershed (Rif, Morocco). *Ecological Engineering & Environmental Technology*, 26(3), 361–377. <https://doi.org/10.12912/27197050/200362>
38. Labriki, A., Chakiri, S., Razoki, B., Bejjaji, Z., Hmidi, F. E., Rassou, K. K. (2019). L'évolution géo-mécanique du massif paléozoïque de la klippe tectonique d'Al Hoceima (Rif, Maroc) par l'analyse des figures d'instabilité et l'interprétation des données géotechniques. *Bulletin de l'Institut Scientifique, Section Sciences de la Terre*, (41), 13–23. http://www.israbat.ac.ma/wp-content/uploads/2019/12/Lakbiri_2019.pdf
39. Labriki, A., Zerdeb, M.A., Majid, I., Chakiri, S., Abbach, J., Bejjaji, Z., El Hmidi, F. (2020). Morphodynamic and Structural Analysis of Tamda Landslide Dam (Middle Atlas, Morocco). *International Journal of Civil Engineering and Technology*, 11(7), 52–65. <https://doi.org/10.34218/IJCET.11.7.2020.006>
40. Labriki, M. (1996). *Carte géologique du Maroc, feuille d'Amez Miz au 1/100 000*. Notes et Mémoires du Serv Géol du Maroc, n° 372.
41. Mattauer, M., Tapponnier, P., Proust, F. (1977). Sur les mécanismes de formation des chaînes intracontinentales. L'exemple des chaînes atlasiques du Maroc. *Bulletin de la Société Géologique de France*, 7, 521–526.
42. Meunier P., Hovius N., Haines J.A. (2008) Topographic site effects and the location of earthquake induced landslides. *Earth Planet Sci Lett* 275: 221–232
43. Michaelides, R.J., Zebker, H.A., Zheng, Y. (2019). An algorithm for estimating and correcting decorrelation phase from InSAR data using closure phase triplets. *IEEE Transactions on Geoscience and Remote Sensing*, 57(12), 10390–10397.
44. Michard A. (1976). *Eléments de géologie marocaine, Notes et Mémoires du Service Géologique du Maroc*, 252, 408. Chalouan, A., Frizon de Lamotte, D. (Eds.), Continental Evolution: The Geology of Morocco. Lecture Notes in Earth Sciences, vol. 116. Springer, Berlin.
45. Morel, J., Zouine, E.-M., Andrieux, J., Faure-Muret, A. (2000). Déformations néogènes et quaternaires de la bordure nord haut atlasique (Maroc) : Rôle du socle et conséquences structurales. *J. Afr. Earth Sci*, 30(1), 119–131.
46. Moret, L. (1931). *Recherches géologiques dans l'Atlas de Marrakech*. Notes Mém. Serv. Géol. Maroc, 18, 262.
47. Mustaphi, H., Medina, F., Jabour, H., Hoepffner, C. (1997). Le bassin du Souss (Zone de faille du Tizi n°Test, Haut Atlas occidental, Maroc): résultat d'une inversion tectonique contrôlée par une faille de détachement profonde. *J. Afr. Earth Sci*. 24, 153–168.
48. Notti, D., Herrera, G., Bianchini, S., Meisina, C., García-Davalillo, J. C., Zucca, F. (2014). A methodology for improving landslide PSI data analysis. *Int J of Remote Sens*, 35(6), 2186–2214. <https://doi.org/10.1080/01431161.2014.889864>
49. Nouayti, A., Moudnib, L.E., Khattach, D. et al. (2024). Seismic synthesis of the Al Haouz earthquake of September 8th, 2023 by integrating gravimetric and aeromagnetic data from the western High Atlas in Morocco. *Model. Earth Syst. Environ*. <https://doi.org/10.1007/s40808-024-02148-3>
50. Ouanaïmi, H. (1989). *Evolution sédimentaire et tectonique de la partie orientale du Massif ancien du Haut Atlas (Maroc)*. Unpubl. PhD thesis. Univ. Sci. Techn. Languedoc (Montpellier II), 402.
51. Petit, J.P. (1976). La zone de décrochement de Tizi n°Test et son fonctionnement depuis le Carbonifère. Thèse 3ème cycle, Université de Montpellier-2, 250.
52. Piqué, A. and Laville, E. (1993). L'ouverture de l'Atlantique central: un jeu en extension des structures paléozoïques, *Comptes Rendus Académie des Sciences Paris 317*, séries II, 1325-1332.
53. Poisson, A., Hadri, M., Milhi, A., Julien, M., Andrieux, J. (1998). The central High Atlas (Morocco). Litho- and chrono-stratigraphic correlations during Jurassic times between Tinjdad and Tounfite. *Mém. Museum Nat. Hist. Nat.*, 179, 237–256.
54. Proust, F. (1973). Étude stratigraphique, pétrographique et structurale du bloc oriental du massif ancien du Haut Atlas (Maroc). *Notes et Mem. Serv. Geol. Maroc*, 34, 15–54.
55. Rahoui, H., Labriki, A., Bejjaji, Z., Chakiri, S. (2024). Impact of climate conditions on the water potential of the River Ansegmir Watershed (Morocco). *Ecological Engineering & Environmental Technology*, 25(10), 107–117. <https://doi.org/10.12912/27197050/191362>
56. Sassa, K., Fukuoka, H., Wang, F., Wang, G. (2007) *Landslides induced by a combined effect of earthquake and rainfall*. Progress in Landslide Science. Springer, Berlin, Heidelberg, 193–207. https://doi.org/10.1007/978-3-540-70965-7_14
57. Scott, C., Lohman, R., Jordan, T. (2017). InSAR constraints on soil moisture evolution after the March 2015 extreme precipitation event in Chile. *Scientific Reports*, 7(1), 1–9.

58. Small, D., Schubert, A. (2022). Guide to ASAR Geocoding (Issue 1.12, Ref: UZH-S1-GC-AD). University of Zurich. Subcontract from Telespazio/Vega IDEAS+. Retrieved from <https://sentinel.esa.int/documents/247904/1653442/Guide-to-Sentinel-1-Geocoding.pdf>
59. Xu, B., Li, Z., Zhu, Y., Shi, J., Feng, G. (2020). Kinematic coregistration of Sentinel-1 TOPSAR images based on sequential least squares adjustment. *IEEE Journal of Selected Topics in Applied Earth Observations and Remote Sensing*, 13, 3083–3093. <https://doi.org/10.1109/JSTARS.2020.3000043>
60. Xu, C., Xu, X., Yao, X. et al. (2014). Three (nearly) complete inventories of landslides triggered by the May 12, 2008 Wenchuan Mw 7.9 earthquake of China and their spatial distribution statistical analysis. *Landslides* 11, 441–461. <https://doi.org/10.1007/s10346-013-0404-6>
61. Yoshihara, N., Umezawa, R. (2023). Combining portable cone penetration test and electrical resistivity tomography to assess residual risks after shallow landslides: a case at the Hokkaido Eastern Iburi earthquake in 2018 in Japan. *Landslides* 20, 2171–2185 <https://doi.org/10.1007/s10346-023-02098-4>
62. Ziraoui, A., Kissi, B., Aaya, H. et al. (2024). Seismic risk assessment, damage estimation, and strengthening of seismic construction standards in Morocco. *J Build Rehabil* 9, 79 <https://doi.org/10.1007/s41024-024-00437-z>